Parity-controlled spin-wave excitations in synthetic antiferromagnets

A. Sud, Y. Koike, S. Iihama, et al.

ARTICLES YOU MAY BE INTERESTED IN

Parity-controlled spin-wave excitations in synthetic antiferromagnets

A. Sud,[1,a)] Y. Koike,[2,3] S. Iihama,[4,5] C. Zollitsch,[1] S. Mizukami,[3,5,6] and H. Kurebayashi[1,7,a)]

AFFILIATIONS

[1] London Centre for Nanotechnology, University College London, 17-19 Gordon Street, London WCH1 0AH, United Kingdom
[2] Department of Applied Physics, Tohoku University, Aoba 6-6-05, Sendai 980-8579, Japan
[3] WPI Advanced Institute for Materials Research, Tohoku University, 2-1-1, Katahira, Sendai 980-8577, Japan
[4] Frontier Research Institute for Interdisciplinary Sciences, Tohoku University, Sendai 980-8578, Japan
[5] Center for Spintronics Research Network, Tohoku University, Sendai 980-8577, Japan
[6] Center for Science and Innovation in Spintronics, Tohoku University, Sendai 980-8577, Japan
[7] Department of Electronic and Electrical Engineering, University College London, London WC1E 7JE, United Kingdom

a) Authors to whom correspondence should be addressed: aakanksha.sud.17@ucl.ac.uk and h.kurebayashi@ucl.ac.uk

ABSTRACT

We report in this study the current-induced-torque excitation of acoustic and optical modes in Ta/NiFe/Ru/NiFe/Ta synthetic antiferromagnet stacks grown on SiO_2/Si substrates. The two Ta layers serve as spin torque sources with the opposite polarizations in both spin currents and Oersted fields acting on their adjacent NiFe layers. This can create the odd symmetry of spatial spin torque distribution across the growth direction, allowing us to observe different spin-wave excitation efficiency from synthetic antiferromagnets excited by homogeneous torques. We analyze the torque symmetry by the in-plane angular dependence of symmetric and anti-symmetric line shape amplitudes for their resonance and confirm the parallel (perpendicular) pumping nature for the acoustic (optical) modes in our devices, which is in stark contrast to the modes excited by spatially homogeneous torques. We also present our macrospin model for this particular spin-torque excitation geometry, which excellently supports our experimental observation. Our results offer capability of controlling spin-wave excitations by local spin-torque sources, and we can explore further spin-wave control schemes based on this concept.

Synthetic antiferromagnets (SyAFs) are an excellent platform to explore novel spintronic and magnonic concepts with coupled magnetic moments.[1,2] Unlike a homogeneously magnetized single-layer ferromagnet, coupled magnetic layers are able to offer rich magnetic states where the competition between interlayer exchange coupling, external field-induced Zeeman interaction, and other magnetic anisotropy terms plays a role. This can expand into their dynamic regimes as the coupled moment nature inherently provides two eigenmodes, acoustic and optical modes,[3–5] where time-dependent components of two coupled moments are oscillating in-phase (acoustic) and out-of-phase (optical) in a spin-flop (canted) regime. These pure magnetic modes have been studied and discussed already around the 1990s, e.g., by Grunberg et al.[6] and Zhang et al.,[7] followed by a number of more recent reports to investigate magnetic dynamics in SyAFs for various topics.[8–18] SyAFs are also a subject of spin–orbit torque (SOT) excitations so far at (or close to) the dc limit,[19–24] and there has been little in

the literature on the use of SOTs for exciting SyAF spin waves at GHz frequencies.

When we excite spin waves by oscillating magnetic fields, the spatial symmetry/profile of microwave excitation determines which spin-wave modes are excited. In the simplest case, a uniform distribution of microwave excitation fields across a magnet can excite the uniform spin-wave mode (wavevector $k = 0$) as well as higher-order spin-wave resonance modes ($k > 0$) with odd index numbers since the spatial profile of the microwave excitation and spin-wave mode amplitude (with phase) matches each other in terms of symmetry. Higher-order spin-wave resonance modes with even index numbers are excluded because the mode overlapping between microwaves and the spin waves becomes zero when it is integrated over the real space. This, in turn, suggests that it should be possible to control the selection rules of spin-wave excitations by designing the spatial profile of excitation fields. Accessing hidden spin-wave states and tailoring spin-wave

excitation efficiency by this approach have not been much explored in the past.

In this Letter, we report our study of spin-wave excitation symmetry control by spatially anti-symmetric spin torques in our SyAF devices. By utilizing local spin excitations due to the spin-Hall effect (SHE) and Oersted fields from adjacent heavy-metal Ta layers, we control the spin-wave excitation nature in the SyAF devices. We observe the torque symmetry of the parallel (perpendicular) pumping configuration of acoustic (optical) modes excited and measured in our devices, which is the signature of the anti-symmetric spin torques for the two coupled moments. We provide analytical expressions for rectification voltages calculated based on the Landau–Lifshitz–Gilbert (LLG) equation for coupled magnetic moments at the macrospin limit. The model equations fully support the torque symmetry that we observed in our experiments and allow us to quantitatively analyze spin–orbit transport parameters such as the spin-Hall angle.

Before describing our experimental results, we here generalize the torque symmetry of optical and acoustic mode excitations (τ_{op} and τ_{ac}). In SyAFs for in-plane field canted conditions, optical and acoustic modes can be generated by adding two individual magnetic moments by using π rotation (C_2 operation) with respect to the applied magnetic field direction.[25] We can combine the excitation terms for each moment by following the same manner and produce the torque expressions for both modes as follows:

$$\tau_{op} = \boldsymbol{m}_1^0 \times (\boldsymbol{B}_1 + C_2\boldsymbol{B}_2) + \boldsymbol{m}_1^0 \times \{\boldsymbol{m}_1^0 \times (\boldsymbol{s}_1 + C_2\boldsymbol{s}_2)\}, \quad (1)$$

$$\tau_{ac} = \boldsymbol{m}_1^0 \times (\boldsymbol{B}_1 - C_2\boldsymbol{B}_2) + \boldsymbol{m}_1^0 \times \{\boldsymbol{m}_1^0 \times (\boldsymbol{s}_1 - C_2\boldsymbol{s}_2)\}. \quad (2)$$

Here, $\boldsymbol{m}_1^0$, $\boldsymbol{B}_1$, $\boldsymbol{B}_2$, $\boldsymbol{s}_1$, and $\boldsymbol{s}_2$ are the time-independent component of magnetization for one of the coupled moments, field-like torque for first and second magnetic moments, and spin polarization causing spin-transfer torques for first and second magnetic moments, respectively. Full derivations of these two torque expressions are available in the supplementary material. These expressions represent the torque symmetry of each mode excitation against the direction of the external magnetic field ($\boldsymbol{B}$). When both moments are excited by uniform spin excitation, namely, with the condition of $\boldsymbol{B}_1 = \boldsymbol{B}_2$ and $\boldsymbol{s}_1 = \boldsymbol{s}_2$, we can arrive at the following conclusions. (i) When $\boldsymbol{B}_1$ and $\boldsymbol{s}_1$ are symmetric for the C_2 rotation, τ_{op} is maximized ($\boldsymbol{B}_1 + C_2\boldsymbol{B}_2 = 2\boldsymbol{B}_1$) and $\tau_{ac} = 0$, and (ii) when $\boldsymbol{B}_1$ and $\boldsymbol{s}_1$ are anti-symmetric for the C_2 rotation, $\tau_{op} = 0$ and τ_{ac} is largest. Here, the meaning of $\boldsymbol{B}_1$ and $\boldsymbol{s}_1$ being symmetric (anti-symmetric) for the C_2 rotation is the condition of $\boldsymbol{B}_1 \| \boldsymbol{B}$ ($\boldsymbol{B}_1 \perp \boldsymbol{B}$), which is, in general, termed as the parallel (perpendicular) pumping configuration in magnetic dynamics. Altogether, we can summarize that under a uniform excitation condition, the optical (acoustic) mode can be excited by the parallel (perpendicular) pumping configuration. In the present study, we take this one step further to control the excitation symmetry by designing the local spin excitation configuration. When m_1 and m_2 experience non-uniform spin excitations, we find from Eqs. (1) and (2) that the perpendicular/parallel pumping nature can be tuned in our experiments. In the extreme case where $\boldsymbol{B}_1 = -\boldsymbol{B}_2$ and $\boldsymbol{s}_1 = -\boldsymbol{s}_2$, we predict that the optical (acoustic) mode is excited by the perpendicular (parallel) pumping configuration. This is because the odd–even parity of the spatial spin excitation is changed, leading to the parity change of excited spin-wave modes with this geometry.

Films with SyAFs used in this study were prepared by magnetron co-sputtering techniques at a base pressure of 3×10^{-7} Pa. The films were grown on thermally oxidized Si substrates with stacking patterns of Ta(5)/NiFe(5)/Ru(0.4 or 0.5)/NiFe(5)/Ta(5), where the number in the brackets represents the thickness in nm. Prior to device fabrication, we characterized these films by vibrating magnetometry techniques to quantify the interlayer exchange coupling strength and to confirm the presence of spin-flop regimes in our films. From these films, rectangular bars with a width (length) of 10 (40) μm were defined by standard photo-lithography techniques and Ar ion milling, prior to another Ti/Au bilayer deposition for preparing a microwave waveguide on top of each bar. We exploit spin-transfer-torque ferromagnetic resonance (STT-FMR) techniques[28,29] in order to excite spin waves in our devices where the Ta layers are the source of spin torques acting on the adjacent NiFe layers individually. Crucially, the spin polarization directions of spin torques in the Ta layers are opposite to each other due to the geometry, which achieves the anti-symmetric profile of these torques (e.g., $\boldsymbol{B}_1 = -\boldsymbol{B}_2$) that we utilize in our study. A schematic of our measurement setup is shown in Fig. 1(a). Vector magnets are used to generate B at various in-plane angles ϕ with respect to the current direction to map out the excitation symmetry in our devices. The SHE[30] in the two Ta layers converts electric currents into spin currents injected into both magnetic layers where spin torques are exerted via the STT mechanism, together with field-like torques by Oersted fields. These cause a time-varying magnetization precession at resonance, producing the time-varying resistance change due to anisotropic magnetoresistance (AMR). As a result, frequency mixing of two time-varying components (i.e., current and resistance) results in a time-independent voltage component that we experimentally measure. As discussed later, we compare our experimental results with analytical solutions obtained from a macrospin model with the LLG equation for coupled magnetic moments.

Both acoustic and optical modes have been clearly identified for different excitation frequencies as shown in Fig. 1(b). The canted nature of synthetic antiferromagnets can be observed by the frequency dependence of resonance for both modes in our sample as shown in Fig. 1(c), indicating the presence of anti-ferromagnetic inter-layer exchange coupling through the Ru layer. The optical (acoustic) mode frequency becomes lower (higher) as B is increased, as predicted by the following solutions of the LLG equation for coupled moments (see the supplementary material): $f_{ac} = (\gamma/2\pi)B\sqrt{1 + (\mu_0 M_s/2B_{ex})}$ and $f_{op} = (\gamma/2\pi)\sqrt{2B_{ex}\mu_0 M_s(1 - (B/2B_{ex})^2)}$, where γ, M_s, μ_0, and B_{ex} are the gyromagnetic ratio, saturation magnetization, free space permeability, and interlayer exchange field, respectively; we notice that there is a very subtle non-linear component for the acoustic mode for the low frequency region which we cannot account for by our macrospin model. In Fig. 1(d), we present our numerical solutions of our eigenvalue problem (see the details in Ref. 18) to show good agreement between experimental observation in our device and model calculations. These demonstrations warrant that we are able to excite and measure both acoustic and optical modes in our SyAF STT-FMR devices with dual spin excitation layers.

Individual curves are further analyzed by the following Lorentzian functions to decompose their symmetric (V_{sym}) and anti-symmetric (V_{asy}) components:
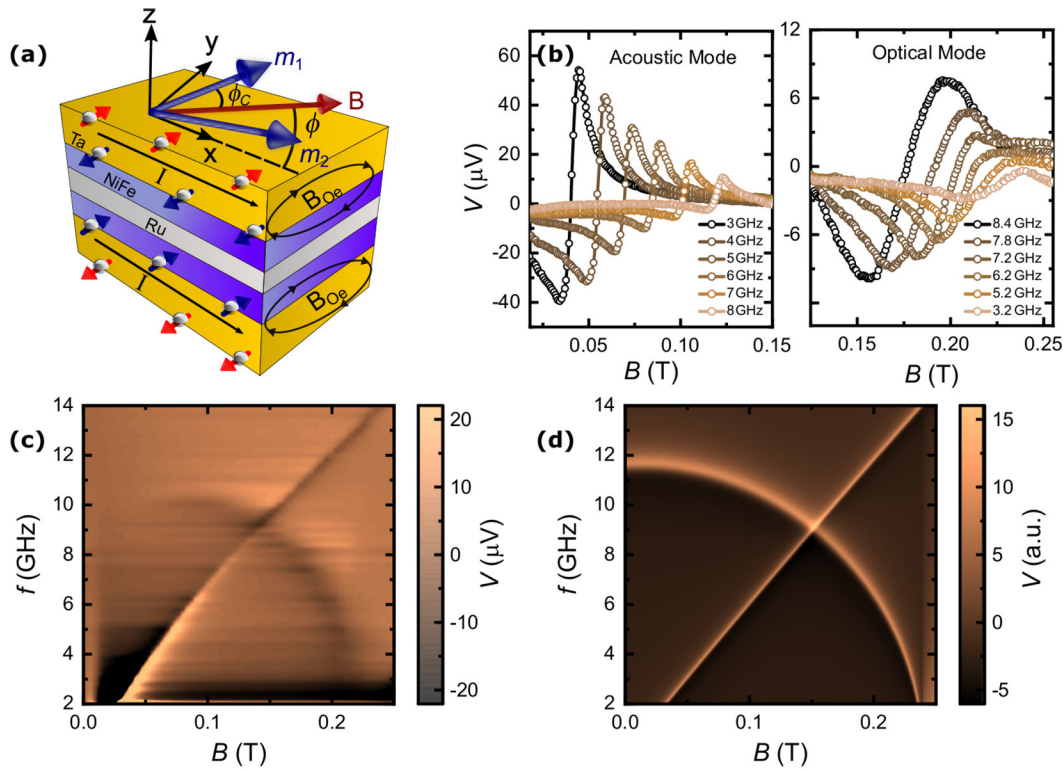
FIG. 1. (a) A schematic of the sample geometry used for STT-FMR measurements in our study. (b) V obtained at different frequencies for acoustic and optical modes in our device for $\phi = 55°$ (the values for some frequencies have been scaled to show them properly). (c) A 2D colorplot of V as a function of applied field and frequency, measured for $\phi = 55°$. (d) Numerical results calculated for the experimental conditions as shown in (d).

$$V_{dc} = V_{sym} \frac{\Delta B^2}{(B - B_{res})^2 + \Delta B^2} + V_{asy} \frac{\Delta B(B - B_{res})}{(B - B_{res})^2 + \Delta B^2}. \quad (3)$$

Here, B_{res} and ΔB are the resonance field and half width at half maximum linewidth of resonance, respectively. Typical FMR curve fit results are shown in Fig. 2(a), which represent excellent fit quality that is also the case for other curve fit analysis throughout this study. Figure 2(b) displays the angular dependence of both V_{sym} and V_{asy} measured for acoustic modes while changing ϕ. Both components clearly show the $\sin 2\phi \sin \phi$ angular dependence, which can be explained by parallel pumping as follows. The angular dependence of observed rectification voltages can be interpreted by the product of the AMR angular dependence ($\sin 2\phi$) and torque symmetry[26,27] (also see the supplementary material). We, therefore, divide both V_{sym} and V_{asy} by $\sin 2\phi$ to reveal the torque symmetry, which is shown in Fig. 2(c) that strongly suggests the torque symmetry for the acoustic mode excitation being the form of $\sin \phi$. This is the case of parallel pumping, i.e., the torque is largest when the applied magnetic field and the oscillating excitation field are collinear ($\phi = 90°$ in our case since both $\boldsymbol{B}_{1,2}$ and $\boldsymbol{s}_{1,2}$ are along this direction). This is remarkably different from the perpendicular pumping nature of acoustic modes in SyAFs, which gives the $\cos \phi$ dependence when they are homogeneously excited as discussed earlier. To determine the efficiency of spin-charge conversion in our devices, we quantified the spin-Hall angle (θ_{SH}) by using the following expression of V_{sym} for the acoustic modes; this is obtained by

solving the LLG equation with coupled moments excited by opposite spin torques at the macrospin limit as shown in the supplementary material,

$$V_{sym} = \frac{-\Delta R_{AMR} C_0 B_{SHE} \cos 2\phi_c \sin \phi_c}{8\Delta B \sqrt{1 + (\mu_0 M_s / 2 B_{ex})} I_0 R_{sample}} P_{input} \sin 2\phi \sin \phi, \quad (4)$$

where B_{SHE} is the field due to the SHE and is defined as $\hbar \eta_{Ta} \theta_{SH} I_0 / 2e M_s w d_{FM} d_{Ta}$. Here, $\hbar$, η_{Ta}, I_0, e, w, d_{FM}, d_{Ta}, ΔR_{AMR}, ϕ_c, P_{input}, R_{sample}, and C_0 refer to the reduced Planck constant, shunt ratio of current in the Ta layer, current amplitude in the device, elementary charge, width of the microbar, thickness of the NiFe and Ta layers, AMR resistance change, cant angle, microwave power at the source, device resistance, and microwave calibration factor to convert the microwave power at the source to that in the device (see the supplementary material), respectively. This equation suggests the linear relationship between V_{sym} and P_{input}, which can be observed in Fig. 2(d). Using the slope fit by the V_{sym} plot and Eq. (4), we extracted the magnitude of θ_{SH} of our Ta layers to be 0.1, which is consistent with previous studies.[31,32] This can strongly suggest that the source of generating V_{sym} in our measurements is due to the SHE in the Ta layers, and we, therefore, conclude that the parallel pumping of SyAF acoustic modes can be achieved by dual spin sources with opposite spin polarization.

We expand our analysis to the optical modes in our devices, which is summarized in Fig. 3. The rectification voltages generated by
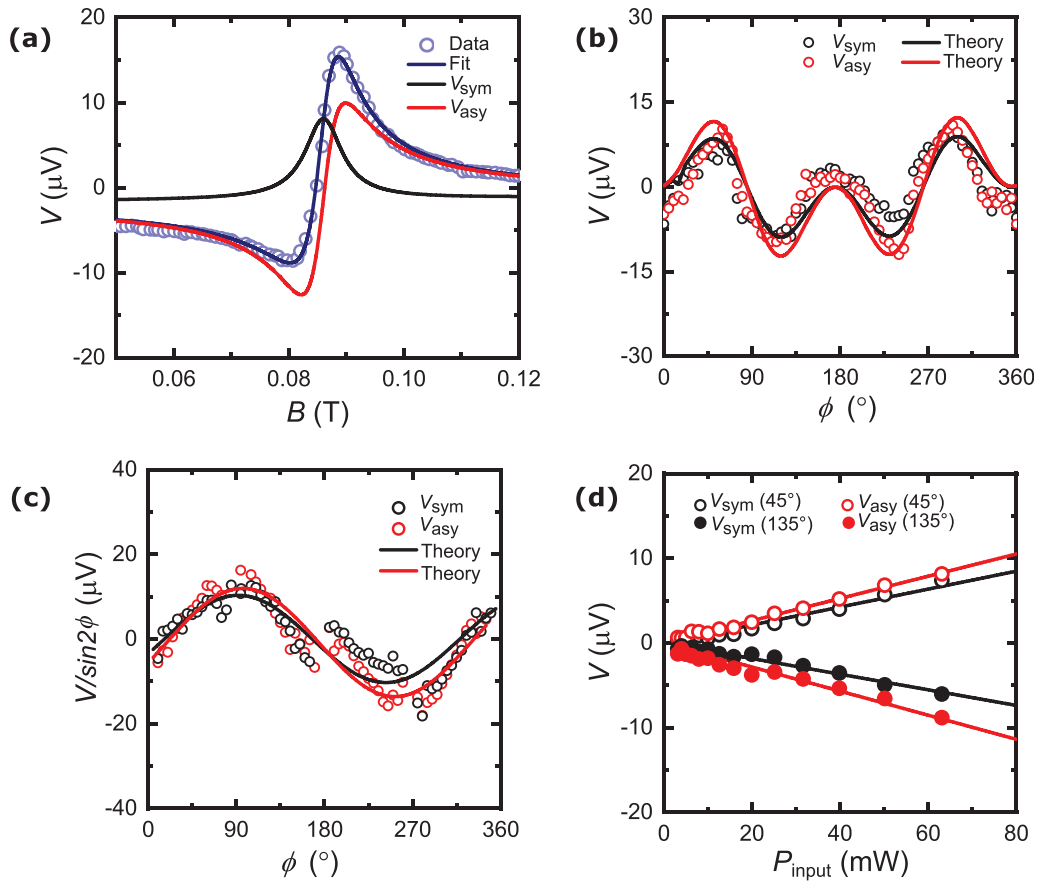
FIG. 2. (a) FMR spectra measured for $f = 6$ GHz and $\phi = 45°$, together with fitting curves produced by using Eq. (3). (b) Angular dependence of V_{sym} and V_{asy} for the acoustic mode measured at 8 GHz. We also add best fit solid curves using our model. (c) The symmetry of torques obtained by dividing the voltage by $\sin 2\phi$. The dominant $\sin \phi$ dependence of torques confirms the parallel pumping configuration. (d) V_{sym} and V_{asy} as a function of P_{input} for $\phi = 45°$ and $135°$ for 8 GHz. The solid lines are linear fit to the data.
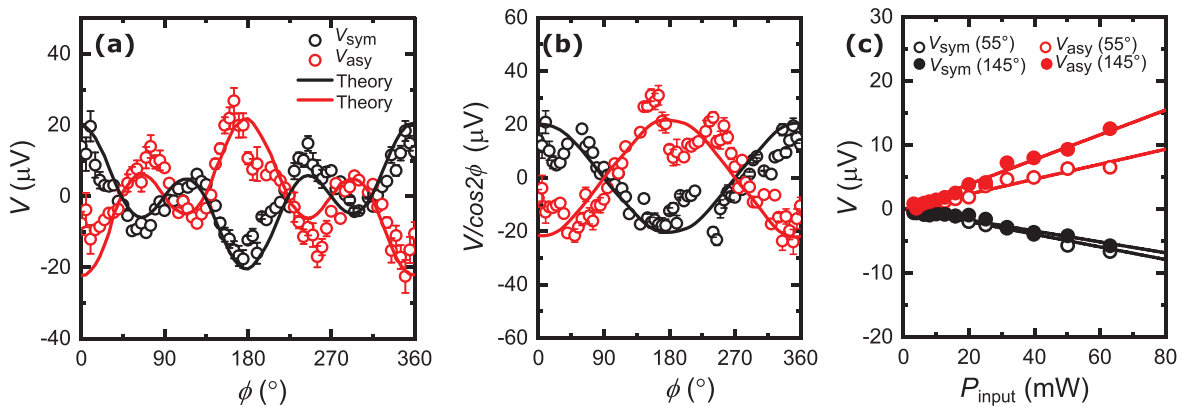

FIG. 3. (a) Angular dependence of V_{sym} and V_{asy} for the optical mode measured at 8.5 GHz. The solid curves are obtained using Eq. (5). (b) The symmetry of torques obtained by dividing the voltage by $\cos 2\phi$. The dominant $\cos \phi$ dependence of torques confirms the perpendicular pumping configuration. (c) The power dependence of V_{sym} and V_{asy} in the optical mode measured at $\phi = 55°$ and $145°$ for $f = 8.5$ GHz, together with linear fit results.

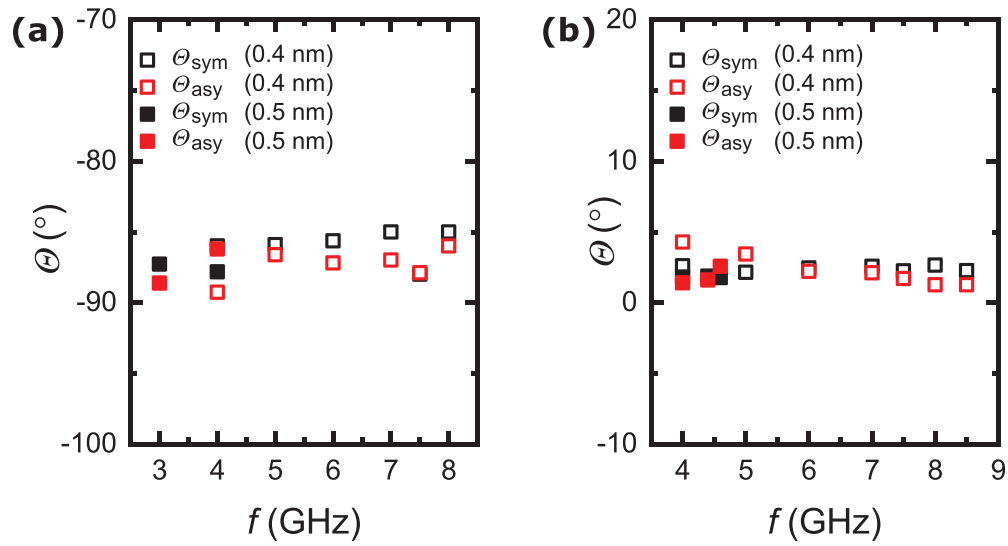**FIG. 4.** Θ extracted as a function of frequency for (a) acoustic and (b) optical modes for different frequencies, in two samples with different Ru thicknesses (0.5 or 0.4 nm). $\Theta_{\text{sym(asym)}}$ represents the parameter extracted from the angular dependence of V_{sym} (V_{asy}) for each frequency. These figures confirm that the acoustic and optical modes are excited by the torque symmetry of parallel and perpendicular pumping configurations, respectively.

optical modes have the following forms (see full derivations in the supplementary material):

$$V_{\text{sym}} = -\frac{\Delta R_{\text{AMR}}}{8\Delta B}\sqrt{\frac{2B_{\text{ex}}}{\mu_0 M_s}}I_0 B_{\text{SHE}}\sin 2\phi_c \sin\phi_c \cos 2\phi \cos\phi,$$

$$V_{\text{asy}} = \frac{\Delta R_{\text{AMR}}}{8\Delta B}I_0 B_{\text{Oe}}\sin 2\phi_c \cos 2\phi \cos\phi. \tag{5}$$

Here, $B_{\text{Oe}} = \mu_0 \eta_{\text{asy}} I_0/2w$ is the Oersted field due to current flowing in the Ta layer with the parameter η_{asy} being the asymmetry factor of electric currents between the Ta and NiFe layers. AMR symmetry for the optical mode is given by $\cos 2\phi$ in these cases, and therefore, we divide experimentally observed V_{sym} and V_{asy} by this to reveal the excitation torque symmetry, which is shown in Fig. 3(b). Unlike the torque symmetry for the acoustic mode [Fig. 2(c)], now we confirm that the symmetry for the optical mode is mainly described by $\cos\phi$, which, in our case, indicates the perpendicular nature of spin-wave excitations, i.e., the torque (hence, spin-wave excitation efficiency) is maximized when the oscillating fields and dc magnetic field are perpendicular to each other. We note that there might be some higher-order terms in this angular dependence that our model cannot capture. However, we emphasize that the main angular dependence in our experiments is clearly reproduced by our model, for both acoustic and optical mode excitations. The sign flip between V_{sym} and V_{asy} for the optical mode, which is predicted by our macrospin model, i.e., in Eq. (5), is also clearly demonstrated in our STT-FMR experiments. θ_{SH} extracted using the slope of our experimental data in Fig. 3(c) is 0.1, showing good agreement with the one extracted by using the acoustic mode resonances.

Finally, we discuss the frequency dependence of the torque symmetry for both modes. In order to quantitatively discuss this, we fit the torque symmetry data [e.g., Fig. 2(c)] by $A\sin\phi + B\cos\phi$ to capture both parallel and perpendicular natures of spin-wave excitations.

Using the prefactors A and B, we define the angle $\Theta = \arctan(A/B)$ that indicates the degree to which spin waves are excited by the parallel or perpendicular pumping configuration; Θ close to $\pm 90°$ ($0°$) suggests the parallel (perpendicular) pumping nature in this definition. We have extracted Θ from our angular dependent measurements and show them in Figs. 4(a) and 4(b) for the acoustic and optical modes, respectively. We observe consistent behaviors of the torque symmetry for both modes as a function of frequency. This confirms the robust parallel (perpendicular) pumping nature of acoustic (optical) modes excited in our SyAF devices with dual spin torque sources using our parity control.

In summary, we demonstrate in this study that local spin torque excitations can convert mode excitation symmetry between perpendicular and parallel pumping configurations in SyAF STT-FMR devices. We show this by using two spin-wave modes, acoustic and optical, both clearly exhibiting the torque symmetry change from the ones expected in spin-wave excitations with homogeneous fields. We also present full expressions of rectification voltages in SyAF STT-FMR devices with dual spin excitations, which support our experimental observation and allow parameter extractions such as the spin-Hall angle using the rectification voltages. We envisage that the control of spin-wave excitations in STT nano-devices will be useful for future spintronic and magnonic nano-devices.

See the supplementary material for our derivations of the torque symmetry of spin-wave excitations and analytical expressions of the rectification voltages based on the macrospin model with coupled LLG equations. It also contains further data of material characterization and additional datasets to support our main claims.

DATA AVAILABILITY

The data that support the findings of this study are available from the corresponding author upon reasonable request.

REFERENCES

[1] R. A. Duine, K.-J. Lee, S. S. P. Parkin, and M. D. Stiles, Nat. Phys. **14**, 217 (2018).

[2] A. V. Chumak, V. I. Vasyuchka, A. A. Serga, and B. Hillebrands, Nat. Phys. **11**, 453–461 (2015).

[3] F. Keffer and C. Kittel, Phys. Rev. **85**, 329 (1952).

[4] J. J. Krebs, P. Lubitz, A. Chaiken, and G. A. Prinz, J. Appl. Phys. **67**, 5920 (1990).

[5] S. M. Rezende, A. Azevedo, and R. L. Rodrguez-Surez, J. Appl. Phys. **126**, 151101 (2019).

[6] P. Grunberg, R. Schreiber, Y. Pang, M. B. Brodsky, and H. Sowers, Phys. Rev. Lett. **57**, 2442 (1986).

[7] Z. Zhang, L. Zhou, P. E. Wigen, and K. Ounadjela, Phys. Rev. B **50**, 6094 (1994).

[8] T. Taniguchi and H. Imamura, Phys. Rev. B **76**, 092402 (2007).

[9] A. Konovalenko, E. Lindgren, S. S. Cherepov, V. Ko-renivski, and D. C. Worledge, Phys. Rev. B **80**, 144425 (2009).

[10] T. Seki, H. Tomita, A. A. Tulapurkar, M. Shiraishi, T. Shinjo, and Y. Suzuki, Appl. Phys. Lett. **94**, 212505 (2009).

[11] T. Chiba, G. E. Bauer, and S. Takahashi, Phys. Rev. B **92**, 054407 (2015).

[12] H. Yang, Y. Li, and W. E. Bailey, Appl. Phys. Lett. **108**, 242404 (2016).

[13] W. Wang, P. Li, P. Cao, F. Liu, R. Tang, G. Chai, and C. Jiang, Appl. Phys. Lett. **113**, 042401 (2018).

[14] A. Kamimaki, S. Iihama, T. Taniguchi, and S. Mizukami, Appl. Phys. Lett. **115**, 132402 (2019).

[15] S. Sorokin, R. A. Gallardo, C. Fowley, K. Lenz, A. Titova, G. Y. P. Atcheson, G. Dennehy, K. Rode, J. Fassbender, J. Lindner, and A. M. Deac, Phys. Rev. B **101**, 144410 (2020).

[16] M. Ishibashi, Y. Shiota, T. Li, S. Funada, T. Moriyama, and T. Ono, Sci. Adv. **6**, eaaz6931 (2020).

[17] Y. Shiota, T. Taniguchi, M. Ishibashi, T. Moriyama, and T. Ono, Phys. Rev. Lett. **125**, 017203 (2020).

[18] A. Sud, C. W. Zollitsch, A. Kamimaki, T. Dion, S. Khan, S. Iihama, S. Mizukami, and H. Kurebayashi, Phys. Rev. B **102**, 100403(R) (2020).

[19] C. Bi, H. Almasi, K. Price, T. Newhouse-Illige, M. Xu, S. R. Allen, X. Fan, and W. Wang, Phys. Rev. B **95**, 104434 (2017).

[20] W. J. Kong, C. H. Wan, X. Wang, B. S. Tao, L. Huang, C. Fang, C. Y. Guo, Y. Guang, M. Irfan, and X. F. Han, Nat. Commun. **10**, 233 (2019).

[21] P. X. Zhang, L. Y. Liao, G. Y. Shi, R. Q. Zhang, H. Q. Wu, Y. Y. Wang, F. Pan, and C. Song, Phys. Rev. B **97**, 214403 (2018).

[22] T. Moriyama, W. Zhou, T. Seki, K. Takanashi, and T. Ono, Phys. Rev. Lett. **121**, 167202 (2018).

[23] Y. Ishikuro, M. Kawaguchi, T. Taniguchi, and M. Hayashi, Phys. Rev. B **101**, 014404 (2020).

[24] H. Masuda, T. Seki, Y.-C. Lau, T. Kubota, and K. Takanashi, Phys. Rev. B **101**, 224413 (2020).

[25] D. MacNeill, J. T. Hou, D. R. Klein, P. Zhang, P. Jarillo-Herrero, and L. Liu, Phys. Rev. Lett. **123**, 047204 (2019).

[26] N. Mecking, Y. S. Gui, and C.-M. Hu, Phys. Rev. B **76**, 224430 (2007).

[27] D. Fang, H. Kurebayashi, J. Wunderlich, K. Výborný, L. P. Zârbo, R. P. Campion, A. Casiraghi, B. L. Gallagher, T. Jungwirth, and A. J. Ferguson, Nat. Nanotechnol. **6**, 413–417 (2011).

[28] A. A. Tulapurkar, Y. Suzuki, A. Fukushima, H. Kubota, H. Maehara, K. Tsunekawa, D. D. Djayaprawira, N. Watanabe, and S. Yuasa, Nature **438**, 339–342 (2005).

[29] L. Liu, T. Moriyama, D. C. Ralph, and R. A. Buhrman, Phys. Rev. Lett. **106**, 036601 (2011).

[30] J. Sinova, S. O. Valenzuela, J. Wunderlich, C. H. Back, and T. Jungwirth, Rev. Mod. Phys. **87**, 1213 (2015).

[31] L. Liu, C.-F. Pai, Y. Li, H. W. Tseng, D. C. Ralph, and R. A. Buhrman, Science **336**, 555 (2012).

[32] E. Sagasta, Y. Omori, S. Vélez, R. Llopis, C. Tollan, A. Chuvilin, L. E. Hueso, M. Gradhand, Y. Otani, and F. Casanova, Phys. Rev. B **98**, 060410(R) (2018).